

Received February 8, 2019, accepted February 22, 2019, date of publication February 28, 2019, date of current version March 18, 2019.

Digital Object Identifier 10.1109/ACCESS.2019.2902315

Imaging With WiFi

STAVROS VAKALIS[®]1, (Student Member, IEEE), LIANG GONG^{1,2}, (Member, IEEE), AND JEFFREY A. NANZER[®]1, (Senior Member, IEEE)

¹Electrical and Computer Engineering Department, Michigan State University, East Lansing, MI 48824, USA
²School of Electrical Engineering and Telecommunications, University of New South Wales Sydney, Sydney, NSW 2052, Australia

Corresponding author: Jeffrey A. Nanzer (nanzer@ieee.org)

This work was supported by the National Science Foundation under Grant 1708820.

ABSTRACT A new method of creating microwave imagery by capturing the signals emitted by a small set of wireless WiFi transmitters is presented. The imaging technique leverages the fact that the signals emitted by separate WiFi transmitters are sufficiently statistically independent to create a radiation pattern that is spatially incoherent, enabling the use of spatial frequency sampling using a small set of receiving antennas in a sparse array. In contrast to traditional microwave imaging, this method requires no mechanical or electrical beam scanning and no coordination between transmitters and receivers. Furthermore, the WiFi imaging system requires far less receiver gain than passive microwave imagers and significantly less bandwidth. We experimentally demonstrate the 2-D image reconstruction of reflecting metal spheres and an X-shaped reflecting target using three transmitters emitting independent 16-level quadrature amplitude modulated signals at 5.5 GHz matching commercial WiFi protocols 802.11n/ac.

INDEX TERMS Computational imaging, interferometry, microwave imaging, radar imaging, Wi-Fi.

I. INTRODUCTION

The use of imagery to convey information has always been widely prevalent in scientific settings and society more broadly due to the inherent human ability to quickly process spatial information. While imagery has traditionally been captured at optical or infrared frequencies, electromagnetic radiation in the microwave and millimeter-wave bands is becoming more widely used for imaging. Wavelengths at these bands are sufficiently small that images can be generated with good resolution, and the signals can easily propagate through smoke, fog, clothing, and even many building materials, which are opaque at optical and infrared wavelengths [1], [2].

Many different techniques of microwave imaging exist, the most common ones being mechanical and electrical scanning imagers [3], which are generally limited by the data acquisition time required to physically scan a beam over a desired field of view. Holographic imaging systems have the same drawback [4]. Staring-type imagers that operate similarly to optical cameras have been developed; examples of these include recently introduced compressive imagers [5], [6], and passive interferometric imagers [7]. The main drawback of compressive imagers is their heavy

The associate editor coordinating the review of this manuscript and approving it for publication was julien Le Kernec.

computational load, and their poor tolerance in low signal-to-noise ratio (SNR) [8]. Passive interferometric imagers employ sparse arrays with fewer elements than a filled aperture [9]; however, because they capture the extremely low power thermal radiation emitted by humans and objects, very high sensitivity receivers are needed with wide bandwidth, leading to high system cost.

The use of WiFi signals for sensing applications has seen significant interest in recent years, due in large part to the ubiquitous presence of WiFi signals from access points in areas where people are present, but also because of the commercial availability of devices that communicate with each other using WiFi protocols [10]. Using WiFi for localization of people and devices [11]-[13], and detection of moving people through walls [14]-[16] have been demonstrated in recent years. While these examples have shown that localization and tracking are possible using WiFi signals, or in some cases using non-communication-type signals in the WiFi bands, the literature on 2-D imaging systems using WiFi still lacks a system that can perform real-time imaging in an affordable fashion. Holography with WiFi has been implemented, but this technique requires either mechanical scanning or a filled 2-D aperture, increasing the total system cost [17]. Other techniques for 2-D and 3-D imaging of scenes require unmanned vehicles to physically coordinate and scan an area or volume, which cannot offer real-time



image reconstruction [18], [19]. In this work we show that the instantaneous wideband nature of WiFi can be beneficial in a sensing application if the receiver and signal processing are appropriately designed, as discussed in the following.

We have developed a new form of microwave computational imaging that uses WiFi signals from separate, independent routers as the transmitters, combined with a sparse array receiver that captures the image information in the spatial frequency domain. Our approach is inspired by passive radar techniques [20], [21], where echoes from third-party radiation is used for target tracking and detection. However, rather than performing traditional radar detection and estimation algorithms, in this imaging system the uncorrelated nature of multiple WiFi signals transmitted from spatially diverse locations enables the use of Fourier-domain spatial sampling to create images. While earlier works on passive imaging systems used sparse arrays [22], [23], such passive systems measure the extremely low-power thermally-generated electromagnetic radiation in the microwave and millimeter-wave bands. To capture this radiation, the receivers must be implemented with very wide bandwidths, in the range of 100s or 1000s of MHz, and very high gains, often exceeding 100 dB, combined with integration times on the order of a few milliseconds to seconds. In previous work, we used independent noise transmitters in order to bypass the wide bandwidth, high sensitivity and long integration time requirements [24]. In this work, by capturing transmitted WiFi signals our approach yields higher received signal power than thermally generated electromagnetic radiation, thus enabling imaging using standard-gain receivers with bandwidths of only 25 MHz and integration time of 10 μ s, both an order of magnitude improvement over the state-of-the-art passive imagers. The result is that the imaging technique presented in this paper can utilize a sparse array with lower-cost commercial hardware compared to other passive techniques and can yield faster image reconstruction. Furthermore, the proposed technique uses existing communications signals in the environment, providing a unique dual-use approach to sensing and communications.

II. INTERFEROMETRIC IMAGE RECONSTRUCTION

The WiFi imaging concept is based on the fact that a 2-D scene can be represented by the superposition of an infinite series of spatial sinusoidally-varying signals of different spatial frequencies. A 2-D antenna array can capture these signals at different spatial frequencies by pairwise cross-correlating the response of its elements. If enough signals corresponding to different spatial frequencies are captured, the scene can be reconstructed in the spatial domain through an inverse Fourier transform (IFT) of the sampled spatial frequency information. First developed in radio astronomy [25], spatial frequency imaging used sparse antenna arrays to capture the thermally generated electromagnetic radiation from astronomical sources and create high-resolution image reconstructions. More recently, this imaging approach has been used in security sensing [7] where

antenna arrays capture the thermal radiation from humans and other objects.

The WiFi imaging system measures spatial-frequency domain information, called *visibility* V(u, v), which is the 2-D Fourier transform of the spatial scene intensity $I(\alpha, \beta)$, with u and v being the two spatial frequency dimensions of the visibility, and $\alpha = \sin\theta\cos\phi$, $\beta = \sin\theta\sin\phi$ are the direction cosines relative to u and v. The two-dimensional visibility is given by

$$V(u, v) = \iint_{-\infty}^{\infty} I(\alpha, \beta) e^{-j2\pi(u\alpha + v\beta)} d\alpha d\beta.$$
 (1)

The imaging process is described in Fig. 1. The signals emitted by a set of WiFi routers or access points reflect off the scene of interest and are captured by a sparse receiving array. Complex data associated with the spatial frequency domain information are captured by processing the received signals in the elements pair-wise. For an antenna pair separated by a baseline D, the spatial frequency is given by $u = D/\lambda$ (rad⁻¹), where λ is the corresponding wavelength. The array captures information residing in a discrete set of two-dimensional spatial frequencies; this set is defined by the pair-wise antenna baselines in two dimensions, and is called the sampling function

$$S(u, v) = \sum_{n=0}^{N} \sum_{m=0}^{M} \delta(u - u_n) \delta(v - v_m)$$
 (2)

where $N \cdot M$ is the maximum number of spatial frequencies (antenna baselines) represented in the array. The sampled visibility $V_s(u, v) = V \cdot S$ is the product of the scene visibility and the sampling function, and represents the information captured by the imaging system.

The Van Cittert-Zernike theorem [27]–[29] indicates that the spatial intensity of a scene I can be reconstructed from samples of the visibility through an inverse Fourier transform providing the signals emitted by the scene are spatially and temporally incoherent. In passive interferometric imaging systems, such as those used in radio astronomy, the signal incoherence constraint is met because the signals are thermally generated by the sources of interest. In this work, the signals transmitted by WiFi routers illuminate the scene of interest. Since each router transmits a different stream of data, and because each router emits signals based on different frequency sources, the resulting signals between multiple routers are largely independent. It can be shown that the radiation from WiFi emissions from multiple routers is sufficiently incoherent by calculating the average spatial mutual coherence of the radiation pattern [30], [31] (commonly used in the compressive sensing field [32]–[34]). The signals thus satisfy the Van Cittert-Zernike theorem, enabling image reconstruction using a simple Fourier transform. To ensure that the signal impinging on the scene is spatially and temporally incoherent, two-dimensional images require three uncorrelated transmitters, ensuring that the signal impinging on the scene is sufficiently uncorrelated in both angular dimensions.

VOLUME 7, 2019 28617



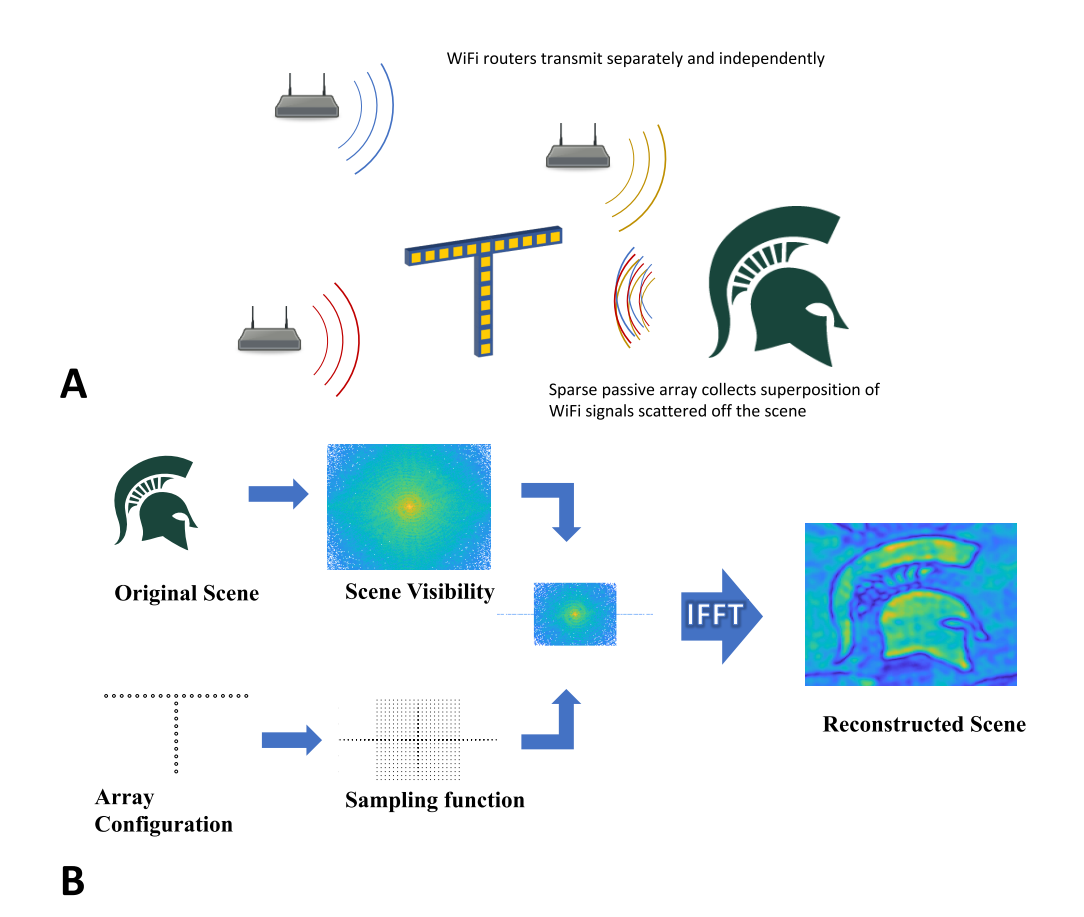


FIGURE 1. (A) Imaging with WiFi signals utilizes a small set of WiFi routers emitting random QAM signals. The receiving array samples the spatial frequency information reflected off the scene on a pair-wise basis. (B) The image is reconstructed by taking the inverse Fourier transform of the sampled scene visibility, the latter being the scene information in the spatial-frequency domain. The sampled visibility is the product of the scene visibility and the sampling function, which is the set of spatial frequencies measured by the array.

With such a transmitter, the received signals are spatially and temporally incoherent, and the reconstructed image I_r is found by

$$I_r(\alpha, \beta) = \sum_{n=1}^{N} \sum_{m=1}^{M} V(u_n, v_m) e^{j2\pi(u_n\alpha + v_m\beta)}.$$
 (3)

The spatial interpretation of this process can be described using the point spread function (PSF) of the array, which can be found through PSF = IFT $\{S(u, v)\}$ and in practice consists of a main beam and a number of sidelobes. The reconstructed image is given by the convolution of the PSF and the scene intensity, $I_r = \text{PSF} * I$.

The spatial resolution of this imaging technique can be approximated using the null-to-null beamwidth of the response from the largest antenna baseline of the receive array in each dimension. For a linear antenna with a largest baseline of D, the null-to-null beamwidth is

$$\theta_{NNBW} \approx 2\frac{\lambda}{D}$$
 (4)

Using x and y to describe the horizontal and vertical axis, the resolution for a two-dimensional array for the two axes

can be defined through

$$\Delta \theta_{x,y} \approx \theta_{NNBW}^{(x,y)} \tag{5}$$

The resolution is only a function of the receive array, however at least three WiFi transmitters are needed in order to ensure that constructive and destructive interference takes place in both the azimuth and elevation planes. The SNR of the received reflections will increase as the number of the WiFi transmitters increases which will contribute to better image reconstruction.

III. INCOHERENCE OF SIGNALS AND THE VAN CITTERT-ZERNIKE THEOREM

To understand why WiFi signals support the incoherence requirement in the Van Cittert-Zernike theorem, one can consider an incoherent radiating source as shown in Fig. 2A, and let its radiation be captured at the two locations of the two antenna elements. The signals received by the antennas are analyzed using the mutual coherence function, which is a measure of the spatial coherence of a signal [25]. In optics, the mutual coherence function for an electric field



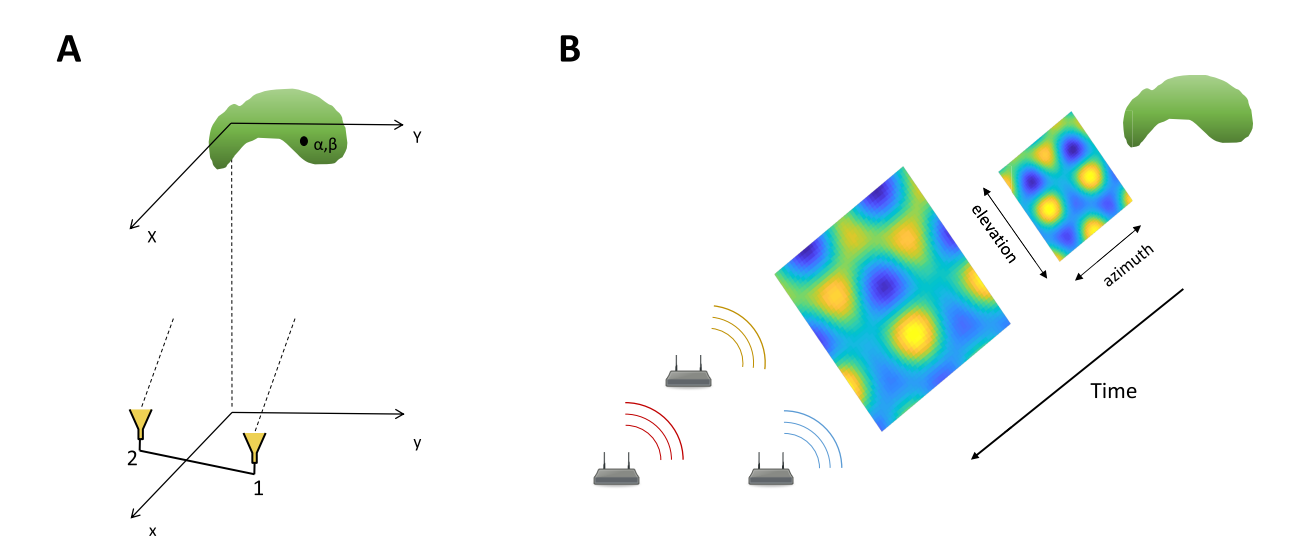


FIGURE 2. (A) Two antenna elements observing a radiating source. (B) Three independent WiFi transmitters illuminating an object. The two slices show the random spatio-temporal transmit pattfern at two separate time instances.

E measured at two different locations 1 and 2, is given by

$$\Gamma_{12}(u, v, \tau) = \lim_{T \to \infty} \frac{1}{2T} \int_{-T}^{T} E_1(t) E_2^*(t - \tau) dt$$
 (6)

where u and v are the electrical coordinates of the spacing between the two measurement points, $u = \frac{(x_1 - x_2)f}{c}$ and $v = \frac{(y_1 - y_2)f}{c}$, where (x_1, y_1) (x_2, y_2) are the locations of elements 1 and 2, f is the carrier frequency, and c is the speed the wavefront propagates. The name of the term suggests that for an incoherent source, observed from a far enough distance, the waves will appear partially coherent.

If the radiating source resides in a much larger distance than the separation of the two elements, then we can assume that the direction cosines α , β (on the azimuth and elevation planes respectively) that an antenna observes the radiating point source through, are the same for both antenna elements 1 and 2 in Fig. 2A. Moreover, the intensities of the received electric fields at both elements can be assumed to be almost the same because they both reside on the same plane, far away from the source. However, the phase term will be time delayed by their distance from the source. As a result, the electric fields resulting from a single point of the source in both the locations 1 and 2 can be given by

$$E_{1}(\alpha, \beta, t) = \mathcal{E}(\alpha, \beta, t) \frac{e^{-j2\pi f(t - R_{1}/c)}}{R_{1}}$$

$$E_{2}(\alpha, \beta, t) = \mathcal{E}(\alpha, \beta, t) \frac{e^{-j2\pi f(t - R_{2}/c)}}{R_{2}}$$
(7)

where $\mathcal{E}(\alpha, \beta, t)$ is the received intensity of the electric field, R_1 , R_2 are the distances of the antenna elements from the point source. By complex cross-correlating the two element responses, a measurement of the common (coherent) signal is given by

$$\langle E_{1}(\alpha, \beta, t) E_{2}^{*}(\alpha, \beta, t) \rangle$$

$$= \langle \mathcal{E}(\alpha, \beta, t) \mathcal{E}^{*}(\alpha, \beta, t) \rangle \frac{e^{-j2\pi f((R_{2} - R_{1})/c))}}{R_{1}R_{2}}$$
(8)

where the angle brackets indicate time-averaging. This quantity thus represents the time-averaged power from the single point source. By integrating over all point sources, the intensity $I(\alpha, \beta)$ of the source can be given in relationship with the mutual coherence of the source at the locations of the two elements by

$$\Gamma_{12}(u, v, 0) = \int_{source} \frac{I(\alpha, \beta)e^{-j2\pi f((R_2 - R_1)/c)}}{R_1 R_2} ds$$
 (9)

where $(R_1 - R_2)$ is the difference in the distances from the point source to locations 1 (x_1, y_1) and 2 (x_2, y_2) . For the amplitude we can assume $R_1 \approx R_2 \approx R$, and $ds = R^2 \, d\alpha d\beta$, thus (6) can be written as

$$\Gamma_{12}(u, v, 0) = \int_{source} I(\alpha, \beta) e^{-j2\pi(u\alpha + v\beta)} d\alpha d\beta. \quad (10)$$

It is clear that that the mutual coherence is the twodimensional Fourier transform of the intensity of the source, which is the definition of the visibility, hence

$$\Gamma_{12}(u, v, 0) = V(u, v).$$
 (11)

IV. INCOHERENCE OF MULTIPLE WIFI SIGNALS USING MUTUAL COHERENCE

To this point, it has been assumed that the point sources composing the source are uncorrelated, generating fully incoherent signals. Thus, after sufficient time averaging, only the correlated signals components remain, and cross-product terms between different points in the form of $\langle E_1(\alpha_i, \beta_i, t)E_2^*(\alpha_j, \beta_j, t)\rangle$ where i and j denote different points of the radiating source, tend to zero. If the radiation from the separate points is not uncorrelated, such cross terms are retained, which make image reconstruction infeasible due to significant interference issues. Thermally radiating sources generate noise-like radiation in both the spatial and temporal domain, and thus the cross terms tend to zero as the integration time increases; this is the reason that passive systems are

VOLUME 7, 2019 28619



unaffected by such terms. However, when the signals being captured are actively transmitted, it is necessary to ensure that the radiation scattered off the scene is sufficiently uncorrelated such that the cross terms still tend to zero. This section is concerned with how an active system can satisfy this requirement when all the sources are not perfectly incoherent and the cross-product terms start to appear, in particular the use of a metric to quantify the spatial incoherence of the scene.

To assess the spatial incoherence of the signals, the fields impinging on the scene, characterized in matrix form ${\bf E}$ with dimensions of time, azimuth plane projection, and elevation plane projection, are analyzed in terms of the coherence between the spatial dimensions of ${\bf E}$. The following analysis is an attempt to quantify the incoherence of the spatio-temporal transmit pattern, and make sure that the dependence between the individual point responses is small. The calculation of electric field is not needed for the image reconstruction. Introduced in optics [28], [29] as the complex degree of coherence, and later in [30] and [31] for sparse representation of signals and matrices, the maximum degree of coherence γ of a matrix ${\bf E}$ with ${\bf K}$ columns and ${\bf T}$ rows is defined as the maximum absolute value of the cross-correlation between the columns of the matrix by

$$\gamma(\mathbf{E}) = \max_{1 \le k \ne j \le K} \frac{|\epsilon_k^H \epsilon_j|}{||\epsilon_k|| ||\epsilon_j||}$$
(12)

where ϵ_k is the k-th column of **E**. In our case K is the number of spatial points of the calculated electric field.

Eq. (12) shows the maximum coherence between two columns of the matrix, corresponding to two spatial points, which as a result is representative of the worst-case. This metric became very popular in the compressive sensing research [32] because if a sensing matrix **E** has low enough mutual coherence the reconstruction of the signal with fewer samples than dictated by the Nyquist criterion will still succeed with high probability. This metric can thus help with comparing the performance of different sensing matrices for sparse representation or reconstruction of signals [33].

Low values of mutual coherence between two vectors correspond to low dependency between them, and both interferometric and compressive imaging systems require an incoherent spatio-temporal pattern for the image reconstruction process to succeed. However, the spatio-temporal pattern for compressive sensing systems needs to be completely known in general, while for the presented imaging system with WiFi signals, the knowledge of the exact transmit pattern is not required as long as it is known to be partially incoherent. Additional spatial variation is also added from the multiple antenna locations that the reflections are measured from. Therefore a more general metric can be adopted, which is the average spatial mutual coherence [34], given by

$$\bar{\gamma}(\mathbf{E}) = \frac{1}{K(K-1)} \sum_{k \to i} \frac{|\epsilon_k^H \epsilon_i|}{||\epsilon_k|| ||\epsilon_j||}$$
(13)

As shown in (10), the average spatial mutual coherence is considerably important because of the integration process that

combines the radiation from multiple single points simultaneously. Low values of average spatial mutual coherence can also be more easily achieved than low values of the maximum degree of coherence. The average value of the cross-correlations between the columns will give a measure of the unwanted information in the image as a result of the superposition of all points on the aperture of the antenna.

To analyze a system using the incoherent radiation from three WiFi transmitters using the average spatial mutual coherence of the spatio-temporal transmit pattern, the transmit pattern is first defined by

$$E(\alpha, \beta, t) = \sum_{l=1}^{3} \int_{f_c - \frac{1}{2}\Delta f}^{f_c + \frac{1}{2}\Delta f} S_l(t) e^{-j2\pi \frac{f}{c}(d_{xl}\alpha + d_{yl}\beta)} df$$
 (14)

where $S_l(t)$ is the 16-QAM signal coming from the l-th transmitter, f_c is the carrier frequency, Δf is the equivalent receiver bandwidth, and the d_{xl} , d_{yl} terms represent the location of the l-th transmitter in the x and y directions accordingly. Fig. 2B shows the spatio-temporal transmit pattern at two separate time instances, making the response of every single point partially independent with each other. The azimuth and elevation planes are noted and the time arrow is pointing towards the transmitters to show that the "frame" furthest away from the transmitters is the one transmitted first.

The spatio-temporal transmit pattern is modeled as described earlier, as a 3-D matrix **E** where the first two dimensions are selected as the two angular dimensions that the antenna array observes the scene from, and the third dimension is time. One may think of the 3-D matrix as a collection of vectors incident to a 2-D plane as shown in Fig. 3A, where only a set of the columns is shown in order to simplify the figure and make it easily understandable. The two azimuth and elevation dimensions indicate the location of every single radiating point. The vertical sets of same color cubes indicate the single point responses over time. To satisfy the Van Cittert-Zernike theorem, the columns in the matrix must be statistically independent.

In order to quantify the independence or incoherence of the columns we use the average spatial mutual coherence metric for a 3-D matrix calculated from (13). The 3-D matrix shown in Fig. 3A can be easily reshaped to 2-D by keeping time as the one dimension and combining the two angle dimensions into one as shown in Fig. 3B. This 3-D to 2-D matrix reshaping is used to speed up computational time and also to keep the paper's structure consistent to the widely used definition of degree of coherence in literature for 2-D matrices. We calculated the spatio-temporal transmit pattern in MATLAB for three random 16-QAM signals modulated on a carrier frequency of 5.5 GHz with 25 MHz of bandwidth. The 3-D spatio-temporal transmit pattern was calculated from (14), and it was transformed from a 3-D matrix into a 2-D matrix, as shown in Fig. 3. The maximum degree of coherence of the matrix, given by (12) was found to be equal to 1, which means that some point sources were coherent, but the average



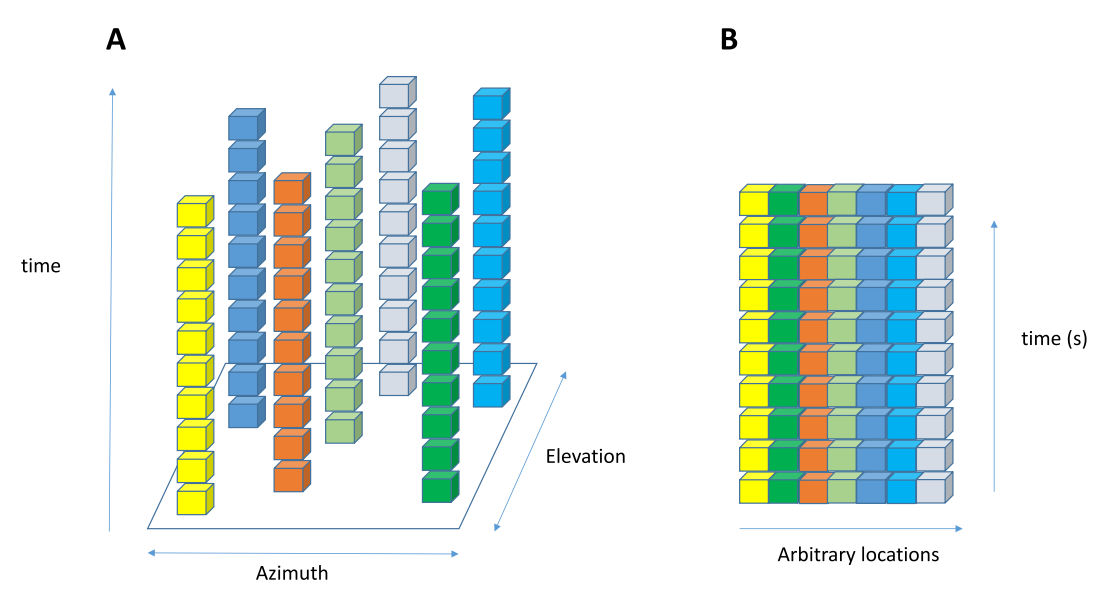


FIGURE 3. (A) The 3-D matrix that represents the incoherent spatio-temporal pattern, where same color represents same point. (B) The 2-D equivalent matrix that resulted from reshaping the 3-D matrix.

spatial mutual coherence, given by (13), was found to be equal to 0.32 for 10 μ s, and by randomizing the locations of the transmitters, this number was very consistent. This means that the normalized coherent part of the radiation coming from two different point sources will be on average less than the one third of the normalized single point response, indicating that the columns are largely independent. This analysis focuses on the transmit pattern and does not take into account the spatial variations when measuring the field in two different locations, for example when two antenna elements are separated by a certain number of wavelengths. Objects in a real scene will add additional unknown amplitude and phase changes randomly in angle, which will further decorrelate the columns of E, and will serve to reduce the average degree of coherence further. Regardless, the following section demonstrates experimental measurements showing that average spatial mutual coherence levels of around 0.32 are sufficient for the WiFi imaging approach.

V. EXPERIMENTAL RESULTS

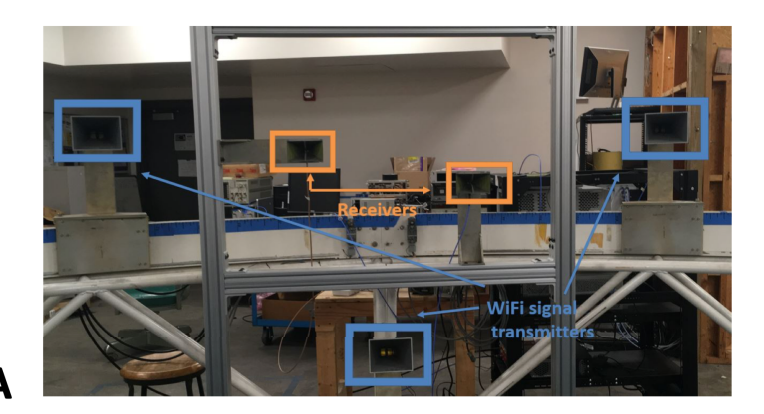
The WiFi imaging system was demonstrated by creating a 2-D experimental setup operating at 5.5 GHz. Since we implemented imaging in two dimensions, three transmitters were used, each emitting pseudo-random 16-QAM signals from 15 dBi antennas. The signals were generated using a Keysight M8190A Arbitrary Waveform Generator, which has only two independent outputs, thus one channel output was split, with one signal fed directly to an antenna and the other delayed through a 7.6 m cable before being fed to another antenna. This additional time delay ensured that the signals incident on the scene were independent and uncorrelated, having the same effect as three independent WiFi transmitters. The scene consisted of two reflecting spheres

placed at the center of a 7.3 m antenna range. For the receive array, we leveraged the fact that each antenna collects spatio-temporally incoherent signals from the scene, enabling us to synthesize a larger aperture by collecting data pairwise with only two receive antennas, and sequentially moving them to the locations of a 2-D inverse T-array. This process yields image formation equivalent to capturing the signals simultaneously in a filled array, since the image information is sampled on a pairwise basis. The configuration for the experimental measurements is shown in Fig. 4A. The receive array had a maximum horizontal dimension of 15λ and a maximum vertical dimension of 8λ, as shown in Fig. 4B, claiming a horizontal and a vertical resolution of 0.13 radians and 0.25 radians respectively. The transmitters were located just outside the span of the receiving array. The received signals were captured using 10 dBi horn antennas, amplified using 20 dB low-noise amplifiers and then downconverted to baseband using quadrature RF mixers. The baseband signals were digitized using a mixed signal oscilloscope and were processed in MATLAB.

The signal processing consisted of digitally low-pass filtering the response of each element to a bandwidth of 25 MHz, then cross-correlating the responses of each antenna pair corresponding to unique spatial frequencies (redundant baselines were omitted) and reconstructing the visibility of the source. The time duration of the captured waveforms was $10~\mu s$, an order of magnitude less than that of typical passive imaging systems, which makes this imaging technique very promising for real-time operation. The reconstructed image was obtained via a 2-D inverse Fourier transform. Fig. 5A shows the two reflecting calibration spheres used for the experimental measurements. The reconstructed image is shown in Fig. 5B, captured pairwise from the locations of the inverse T-array. Fig. 5C shows the deconvolved image

VOLUME 7, 2019 28621





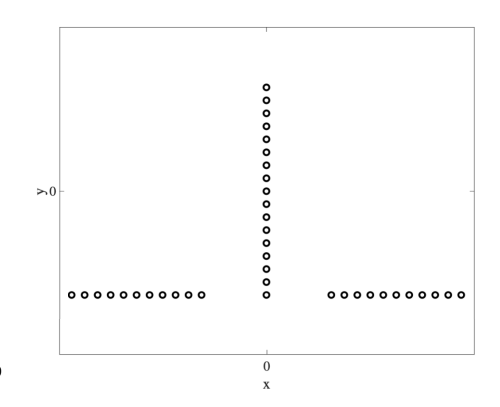


FIGURE 4. (A) Configuration for the experimental 5.5 GHz measurements with three transmitters and two receivers synthesizing a $15\lambda x8\lambda$ array by moving the receiving antennas in the horizontal and vertical directions. (B) The locations of the synthesized array in $\lambda/2$ increments. The narrow baselines are missing due to the dimensions of the horn antennas.

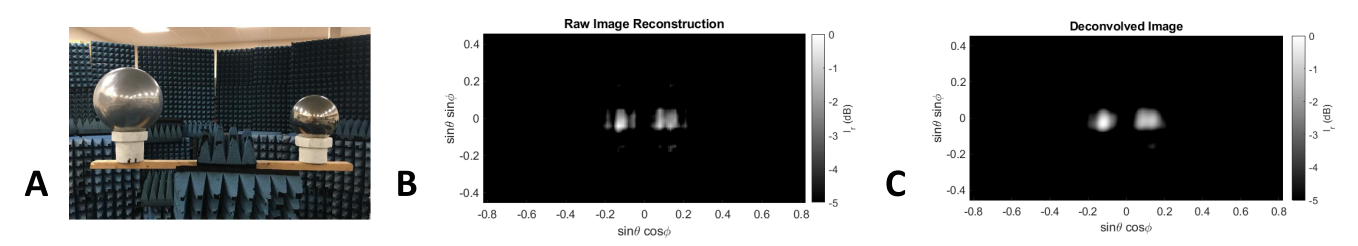


FIGURE 5. (A) The two reflecting calibration spheres used as the two-dimensional scene. (B) Raw reconstructed 5.5 GHz image of the intensities of two reflecting spheres, using data from a full array consisting of all receiver locations. (C) Deconvolved image using the calculated PSF, in which the two responses can be clearly distinguished. The reconstructions are normalized to their peak value, thus the colorbar values are in dB.

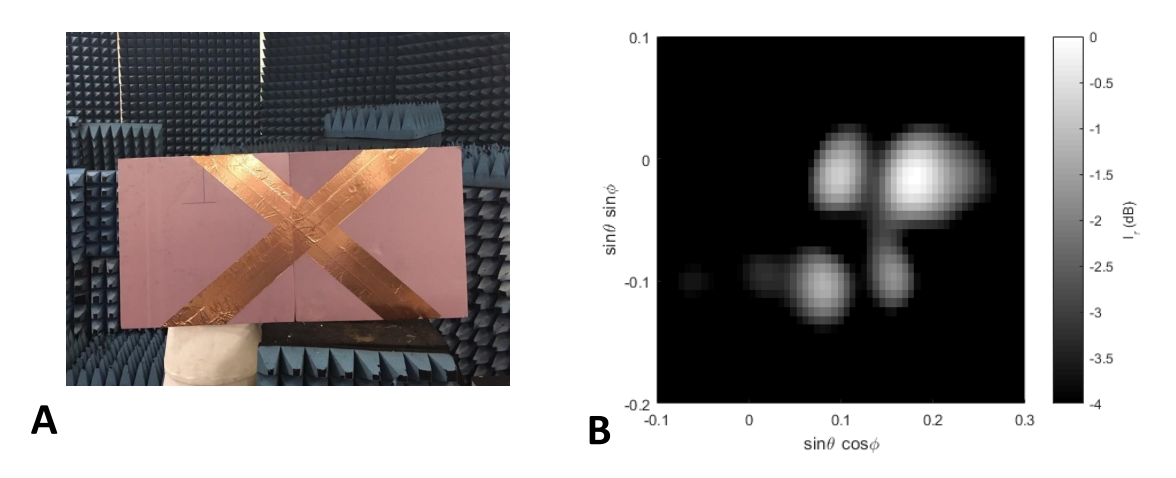


FIGURE 6. (A) The reflecting X-shaped target used as a distributed scene with features smaller than the array resolution.
(B) Reconstructed 5.5 GHz image of the reflecting X-shaped target, using data from a full array consisting of all receiver locations. Although this target is more challenging to image with the given resolution, its features can be distinguished. The reconstruction is normalized to its peak value, thus the colorbar values are in dB.

using blind deconvolution [35] with the calculated PSF of the array shown in Fig. 4B. The responses from the two spheres are clearly distinguishable. A more complex target is shown in Fig. 6A, with an X-shape formed from copper tape on a foam board. The X has edges of 94 cm and 97 cm, however the features are lower than the resolution of the 5.5 GHz imaging array. The array configuration used for the calibration

spheres was used for imaging the X, with the result shown in Fig. 6B. The overall shape of the X is clearly apparent, with bright spots aligning with the arms of the X. There is some loss of the shape between the bright responses, however the overall shape is clearly distinguished, demonstrating the feasibility of imaging complex objects using 5.5 GHz WiFi signals.



VI. SUMMARY AND CONCLUSION

The imaging technique presented in this paper is the first to generate imagery in two angle dimensions using WiFi signals as the illuminators. Furthermore, no connection between the receivers and transmitters is required, with the only necessary information being the statistics of the transmitted signals. Using this technique, full 2-D imagery is possible by capturing the WiFi signals present in typical environments, using calibration spheres and more challenging distributed targets. Due to the ability of WiFi to propagate through building materials, the potential for through-wall imaging using ambient WiFi signals exists. With the first 802.11ad commercial routers, operating at 60 GHz, being already available and enabling even higher resolution, future implementations may yield images with significant resolution capabilities.

REFERENCES

- [1] J. Nanzer, Microwave and Millimeter-Wave Remote Sensing for Security Applications. Norwood, MA, USA: Artech House, 2012.
- [2] N. C. Currie and C. E. Brown, Principles and Applications of Millimeter-Wave Radar. Norwood, MA, USA: Artech House, 1987.
- [3] S. S. Ahmed, A. Schiessl, and L.-P. Schmidt, "A novel fully electronic active real-time imager based on a planar multistatic sparse array," *IEEE Trans. Microw. Theory Techn.*, vol. 59, no. 12, pp. 3567–3576, Dec. 2011.
- [4] D. M. Sheen, D. L. McMakin, and T. E. Hall, "Three-dimensional millimeter-wave imaging for concealed weapon detection," *IEEE Trans. Microw. Theory Techn.*, vol. 49, no. 9, pp. 1581–1592, Sep. 2001.
- [5] J. Hunt et al., "Metamaterial apertures for computational imaging," Science, vol. 339, no. 6117, pp. 310–313, Jan. 2013.
- [6] J. Romberg, "Imaging via compressive sampling," *IEEE Signal Process. Mag.*, vol. 25, no. 2, pp. 14–20, Mar. 2008.
- [7] L. Yujiri, M. Shoucri, and P. Moffa, "Passive millimeter wave imaging," IEEE Microw. Mag., vol. 4, no. 3, pp. 39–50, Sep. 2003.
- [8] M. A. Davenport, J. N. Laska, J. R. Treichler, and R. G. Baraniuk, "The pros and cons of compressive sensing for wideband signal acquisition: Noise folding versus dynamic range," *IEEE Trans. Signal Process.*, vol. 60, no. 9, pp. 4628–4642, Sep. 2012.
- [9] A. Moffet, "Minimum-redundancy linear arrays," *IEEE Trans. Antennas Propag.*, vol. 16, no. 2, pp. 172–175, Mar. 1968.
- [10] W. Xu, H. A. Omar, W. Zhuang, and X. S. Shen, "Delay analysis of invehicle Internet access via on-road WiFi access points," *IEEE Access*, vol. 5, pp. 2736–2746, 2017.
- [11] S. Kumar, S. Gil, D. Katabi, and D. Rus, "Accurate indoor localization with zero start-up cost," in *Proc. 20th Annu. Int. Conf. Mobile Comput. Netw.*, Sep. 2014, pp. 483–494.
- [12] M. Kotaru, K. Joshi, D. Bharadia, and S. Katti, "SpotFi: Decimeter level localization using WiFi," in *Proc. ACM Conf. Special Interest Group Data Commun.*, New York, NY, USA, Aug. 2015, pp. 269–282.
- [13] Y. Xie, Y. Zhang, J. C. Liando, and M. Li, "SWAN: Stitched Wi-Fi ANtennas," Proc. 24th Annu. Int. Conf. Mobile Comput. Netw., Oct./Nov. 2018, pp. 51–66.
- [14] F. Adib, D. Katabi, "See through walls with WiFi!" in *Proc. ACM SIG-COMM Conf. SIGCOMM*, New York, NY, USA, Aug. 2013, pp. 75–86.
- [15] K. Chetty, G. E. Smith, and K. Woodbridge, "Through-the-wall sensing of personnel using passive bistatic WiFi radar at standoff distances," *IEEE Trans. Geosci. Remote Sens.*, vol. 50, no. 4, pp. 1218–1226, Apr. 2012.
- [16] Y. Zhu et al. (2018). "Adversarial WiFi sensing using a single smartphone." [Online]. Available: https://arxiv.org/abs/1810.10109
- [17] P. M. Holl and F. Reinhard, "Holography of Wi-Fi radiation," *Phys. Rev. Lett.*, vol. 118, no. 18, May 2017, Art. no. 183901.
- [18] S. Depatla, L. Buckland, and Y. Mostofi, "X-ray vision with only WiFi power measurements using rytov wave models," *IEEE Trans. Veh. Tech*nol., vol. 64, no. 4, pp. 1376–1387, Apr. 2015.

- [19] C. R. Karanam and Y. Mostofi, "3D through-wall imaging with unmanned aerial vehicles using WiFi," in *Proc. 16th ACM/IEEE Int. Conf. Inf. Process. Sensor Netw. (IPSN)*, Pittsburgh, PA, USA, Apr. 2017, pp. 131–142.
- [20] P. E. Howland, D. Maksimiuk, and G. Reitsma, "FM radio based bistatic radar," *IEE Proc.- Radar, Sonar Navigat.*, vol. 152, no. 3, pp. 107–115, Jun. 2005.
- [21] C. R. Berger, B. Demissie, J. Heckenbach, P. Willett, and S. Zhou, "Signal processing for passive radar using OFDM waveforms," *IEEE J. Sel. Topics Signal Process.*, vol. 4, no. 1, pp. 226–238, Feb. 2010.
- [22] H. Nohmi, S. Ohnishi, and O. Kujubu, "Passive millimeter-wave camera with interferometric processing," *Proc. SPIE*, vol. 6548, pp. 65480C-1–65480C-8, May 2007.
- [23] N. A. Salmon, A. Harvey, and C. Taylor, "First video rate imagery from a 32-channel 22-GHz aperture synthesis passive millimetre wave imager," *Proc. SPIE*, vol. 8188, Oct. 2011, Art. no. 5.
- [24] S. Vakalis and J. A. Nanzer, "Microwave imaging using noise signals," IEEE Trans. Microw. Theory Techn., vol. 66, no. 12, pp. 5842–5851, Dec. 2018.
- [25] A. R. Thompson, J. M. Moran, and G. W. Swenson, Jr., Interferometry and Synthesis in Radio Astronomy. New York, NY, USA: Wiley, 2001.
- [26] B. F. Burke and F. Graham-Smith, An Introduction to Radio Astronomy. Cambridge, U.K.: Cambridge Univ. Press, 2002.
- [27] P. H. van Cittert, "Die wahrscheinliche schwingungsverteilung in einer von einer lichtquelle direkt oder mittels einer linse beleuchteten ebene" *Physica*, vol. 1, nos. 1–6, pp. 201–210, 1934.
- [28] F. Zernike, "The concept of degree of coherence and its application to optical problems," *Physica*, vol. 5, no. 8, pp. 785–795, Aug. 1938.
- [29] M. Born and E. Wolf, Principles of Optics: Electromagnetic Theory of Propagation, Interference and Diffraction of Light. Cambridge, U.K.: Cambridge Univ. Press, 1999.
- [30] D. L. Donoho and X. Huo, "Uncertainty principles and ideal atomic decomposition," *IEEE Trans. Inf. Theory*, vol. 47, no. 7, pp. 2845–2862, Nov. 2001.
- [31] D. L. Donoho and M. Elad, "Optimally sparse representation in general (nonorthogonal) dictionaries via l¹ minimization," *Proc. Nat. Acad. Sci.* USA, vol. 100, no. 5, pp. 2197–2202, 2003.
- [32] E. J. Candès and M. B. Wakin, "An introduction to compressive sampling," *IEEE Signal Process. Mag.*, vol. 25, no. 2, pp. 21–30, Mar. 2008.
- [33] R. Obermeier and J. A. Martinez-Lorenzo, "Sensing matrix design via mutual coherence minimization for electromagnetic compressive imaging applications," *IEEE Trans. Comput. Imag.*, vol. 3, no. 2, pp. 217–229, Jun. 2017.
- [34] J. M. Duarte-Carvajalino and G. Sapiro, "Learning to sense sparse signals: Simultaneous sensing matrix and sparsifying dictionary optimization," *IEEE Trans. Image Process.*, vol. 18, no. 7, pp. 1395–1408, Jul. 2009.
- [35] D. Kundur and D. Hatzinakos, "Blind image deconvolution," *IEEE Signal Process. Mag.*, vol. 13, no. 3, pp. 43–64, May 1996.



STAVROS VAKALIS (S'18) received the B.S. degree in electrical and computer engineering from the National Technical University of Athens, Athens, Greece, in 2017. He is currently pursuing the Ph.D. degree in electrical engineering with Michigan State University, East Lansing, MI, ISA

His current research interests include wireless microwave and millimeter-wave systems, antenna arrays, radars, and signal processing.





LIANG GONG (S'12–M'17) received the B.Eng. degree in electrical engineering from Xidian University, Xi'an, China, in 2008, the M.Eng.Sc. and Ph.D. degrees from the University of New South Wales (UNSW) Sydney, Sydney, Australia, in 2013 and 2017, respectively. In 2012, he joined the Microsystems Research Group, School of Electrical Engineering and Telecommunications, (UNSW) Sydney. He is currently a Postdoctoral Research Associate with the Department of Elec-

trical and Computer Engineering, Michigan State University, East Lansing, MI, USA, jointly with UNSW Sydney. His research interests include the RF MEMS, antennas, millimeter-wave circuits and systems, radar, and interferometric imaging systems.



JEFFREY A. NANZER (S'02–M'08–SM'14) received the B.S. degree in electrical engineering and computer engineering from Michigan State University, East Lansing, MI, USA, in 2003, and the M.S. and Ph.D. degrees in electrical engineering from The University of Texas at Austin, Austin, TX, USA, in 2005 and 2008, respectively. From 2008 to 2009, he was a Postdoctoral Fellow with Applied Research Laboratories, The University of Texas at Austin, where he was

involved in designing electrically small HF antennas and communication systems. From 2009 to 2016, he was with The Johns Hopkins University Applied Physics Laboratory, Laurel, MD, USA, where he created and led the Advanced Microwave and Millimeter-Wave Technology Section. In 2016, he joined the Department of Electrical and Computer Engineering, Michigan State University, where he is currently a Dennis P. Nyquist Assistant Professor. He has authored or co-authored more than 80 refereed journal and conference papers, authored Microwave and Millimeter-Wave Remote Sensing for Security Applications (Artech House, 2012), and co-authored the chapter "Photonics-Enabled Millimeter-Wave Wireless Systems" in Wireless Transceiver Circuits (Taylor and Francis, 2015). His current research interests include distributed arrays, radar and remote sensing, antennas, electromagnetics, and microwave photonics.

Dr. Nanzer is a Member of the IEEE Antennas and Propagation Standards Committee, the AP-S Education Committee, and the USNC/URSI Commission B. He was a Founding Member and the First Treasurer of the IEEE APS/MTT-S Central Texas Chapter. He was a recipient of the NSF CAREER Award, in 2018, the DARPA Young Faculty Award, in 2017, JHU/APL Special Achievement Awards, in 2014 and 2016, and the JHU/APL Outstanding Professional Book Award, in 2012. From 2013 to 2015, he served as the Vice-Chair of the IEEE Antenna Standards Committee. From 2016 to 2018, he was the Chair of the Microwave Systems Technical Committee (MTT-16), IEEE Microwave Theory and Techniques Society. He is currently an Associate Editor of the IEEE Transactions on Antennas and Propagation.

0 0 0